Communication

Heterogeneous Nucleation of Eutectic Structure in Al-Mg-Si Alloys

ZHONGPING QUE, YUN WANG, and ZHONGYUN FAN

The microstructure of Al-5Mg-2Si-0.4Mn-0.7Fe alloy solidified at different conditions were examined. Different kinds of eutectic structures such as ($Al_{15}(Fe,Mn)_3Si_2$ + α-Al), (Mg_2Si + α-Al) and (FIMCs + Mg_2Si + α-Al) were selected due to the different primary phases formation. The phase relationships between the phases within the eutectic structures, and the phase relationships between the primary phases and the eutectic leading phases were investigated. A well-defined orientation relationship (OR) between α-$Al_{15}(FeMn)_3Si_2$ and Mg_2Si was examined.

https://doi.org/10.1007/s11661-020-05735-y

Aluminium alloys with fine grain structure have received great attention in various fields especially in automotive and aerospace industries due to the advanced properties such as low density and good castability.[1,2] Grain refinement of Al alloys not only can reduce casting defects such as hot tearing and porosity but also can enhance mechanical properties such as strengths and ductility.[3] Many kinds of grain refinement methods were developed, such as thermal control,[4] chemical methods,[5,6] and mechanical method.[7] One of the most successful ways to grain refine Al alloys by chemical method during the casting process is development of Al-Ti-B master alloy system as effective grain refiners.[5,6,8] The master alloys significantly refined α-Al grains by providing extra Ti or B and TiB_2 particles as the inoculants for different Al alloys.[9,10]

However, all these grain refinement methods are focusing on the refinement of α-Al grains. The other very important factor for the mechanical properties is eutectic structure in the Al alloys. In most of Al alloys, the eutectic structures consist of α-Al phase with one or more kinds of intermetallic compounds (IMCs). The eutectic spacing, eutectic grain size, the size and morphology of the IMCs play very important roles in determining the mechanical properties. As reported,[11,12] the eutectic structures in Al alloys were difficult to control and unpredictable due to the composition segregation. Therefore, to achieve high mechanical properties for Al alloys, the refinement of eutectic structure is as important as the α-Al grain refinement. For example, as one of the unavoidable impurities in Al alloys, Fe usually forms large-scale Fe-containing IMCs.[13–19] These FIMCs deteriorate the mechanical properties especially the toughness when they have the large plate-like or needle-like shapes.

Recent research[20] indicated that the solidification sequence affected the formation of FIMCs in the eutectic structure. Therefore, a better understanding on nucleation of the eutectic in Al alloys should be brought to the attention for controlling the eutectic structure. In this study, we aimed to investigate the nucleation of the leading phase of eutectic structure during the solidification process of Al alloys. The microstructure variation due to the leading phase changes under different solidification conditions was studied as well.

The alloy used in this study had a composition of 5.66 ± 0.6 Mg, 2.65 ± 0.2 Si, 0.44 ± 0.2 Mn, 0.67 ± 0.2 Fe and balanced Al (all compositions are in wt pct unless specified otherwise). The phase diagram of the Al-5Mg-2Si-0.4Mn-0.7Fe alloy was calculated by Pandat software with Sheil model. The liquidus for the alloy was 638.34 °C, and the main solidification sequence is primary $Al_{15}(Fe,Mn)_3Si_2$, binary eutectic ($Al_{15}(Fe,Mn)_3Si_2$ + α-Al), and ternary eutectic (α-Al + $Al_{13}Fe_4$ + Mg_2Si).

Pure Al (> 99.86 pct), Pure Mg (> 99.95 pct), Al-50 pct Si, Al-20 pct Mn and Al-38 pct Fe master alloys were used to prepare the alloy with the above nominal composition. The standard TP-1 test[21] was used to assess the solidified microstructure of the alloy under a fixed solidification condition with a cooling rate of 3.5 K/s. The prepared alloy melt was isothermally held at 750 °C for 30 minutes in an electric resistance furnace, and then cast into the TP-1 mould. The pouring temperature for the TP-1 test of the alloy melt was 660 °C and 690 °C.

The microstructure characteristics of the samples were examined using a Zeiss field emission gun (FEG) Supra 35 scanning electron microscope (SEM). To investigate the 3-dimensional morphology of the IMCs, samples were deep-etched in an etchant of an aqueous solution containing 10 to 15 vol pct HCl for 1 to 3 minutes. After dissolution of the Al matrix in 1 to 2 mm thick, the remaining was treated with completely but gently cleaning in an ethanol bath to get rid of the etching solution. The EBSD measurements were made using the Zeiss Crossbeam 340 FIB instrument. The scanning step

ZHONGPING QUE, YUN WANG, and ZHONGYUN FAN are with the BCAST, Brunel University London, Uxbridge, Middlesex UB8 3PH, UK, Contact e-mail: Zhongping.Que@brunel.ac.uk
Manuscript submitted October 10, 2019.
Article published online March 30, 2020

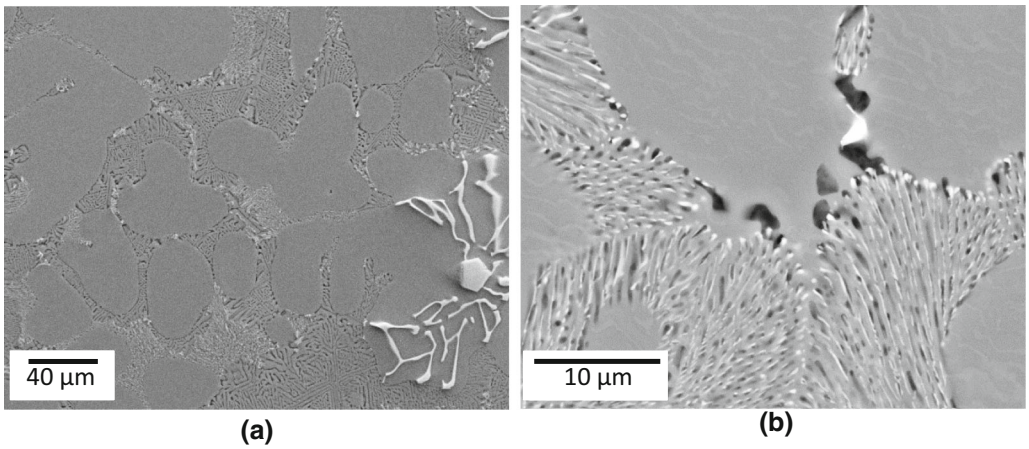

Fig. 1—Backscattered electron SEM images showing the microstructure of Al-5Mg-2Si-0.4Mn-0.7Fe alloys solidified at 3.5 K/s with pouring temperature of (*a*) 690 °C indicating the microstructure with Chinese script binary eutectic (FIMCs + α-Al), primary α-Al and ternary eutectic, and (*b*) 660 °C showing the TE-(FIMCs + α-Al + Mg_2Si) structure associated with primary α-Al. In the SEM-BSD (backscattered electron detector) images, the FIMCs were shown in white, Mg_2Si in black, and α-Al in grey.

size ranged from 0.05 to 0.2 μm. Thin foils for high-resolution transmission electron microscopy (HRTEM) examinations were prepared from the slices of different samples which were cut into 3 mm diameter discs and finally grounded to a thickness of less than 60 μm, followed by ion-beam-thinning using a Gatan precision ion polishing system (PIPS) at an energy of 3 to 5.0 kV and an incident angle of 3 to 6 deg. TEM examination was performed on a JEOL 2100F microscope equipped with EDS facility operated at an accelerating voltage of 200 kV.

Figure 1(a) demonstrates a microstructure consisting of the primary FIMC with compacted morphology, the binary eutectic (BE) (FIMC + α-Al) and/or binary eutectic (Mg_2Si + α-Al) with Chinese script morphology, the primary α-Al and the ternary eutectic (TE) (FIMCs + Mg_2Si + α-Al) when casted at 690 °C. It demonstrates that the BE-(FIMC + α-Al) and BE-(Mg_2Si + α-Al) structures are coarse and only a small amount TE-(FIMCs + Mg_2Si + α-Al) can be examined. The eutectic spacing of BE-($Al_{15}(Fe,Mn)_3Si_2$ + α-Al) and BE-(Mg_2Si + α-Al) were quantified to be 12.2 ± 1.0 and 2.0 ± 0.2 μm. The measurement for the BE structure with Chinese script morphology was done according to the secondary dendritic arm spacing of the intermetallic compounds. All the phases were identified with the SEM and EBSD analysis. The FIMCs in the primary and binary eutectic structures were identified as $Al_{15}(Fe,Mn)_3Si_2$. The black phase in the Chinese script BE structure was identified as Mg_2Si. The small amount white phase in the TE structure was identified as major $Al_{13}Fe_4$ mixed with some $Al_{15}(Fe,Mn)_3Si_2$ by TEM analysis.

Figure 1(b) shows that no primary FIMCs can be observed, and the primary α-Al is dominating. The structure surrounding the primary α-Al dendrites is the TE-(FIMCs + Mg_2Si + α-Al) with a very fine spacing (0.62 ± 0.05 μm) which is much smaller than that of the Chinese script BE structures. The intermetallic compounds in these TE structure presents the needle-like morphology. The white IMC is identified as $Al_{13}Fe_4$, and the black IMC is identified as Mg_2Si.

The 3D morphology shown in Figure 2(a) demonstrates that the Chinese script $Al_{15}(Fe,Mn)_3Si_2$ phase connected and grown from the compacted primary $Al_{15}(Fe,Mn)_3Si_2$ phase, with the latter being identified as the nucleation substrate for the $Al_{15}(Fe,Mn)_3Si_2$ phase in BE structure.[20] The eutectic associated to the BE-($Al_{15}(Fe,Mn)_3Si_2$ + α-Al) is the Chinese script BE-(Mg_2Si + α-Al).

Figure 2(b) shows 3D morphology of the TE structure in the α-Al inter-dendritic zone. After deep etching, the α-Al and Mg_2Si phase in the TE structure are almost gone. The remaining phase in the TE structure is the $Al_{13}Fe_4$ phase. It shows that the TE-$Al_{13}Fe_4$ phase is fine and has needle-like morphology.

The orientation relationships between the primary phases ($Al_{15}(Fe,Mn)_3Si_2$ or α-Al) and its surrounding eutectic structures are examined by EBSD. Our previous work[20] has proved that the Chinese script BE-$Al_{15}(Fe,Mn)_3Si_2$ was nucleated from the connected compacted primary $Al_{15}(Fe,Mn)_3Si_2$. Therefore, in this study, we focus on the relationship between the primary α-Al and the associated BE structures.

Figures 3(a) through (c) show the EBSD mapping results of Chinese script BE structures in sample that casted at 690 °C. Figure 3(a) shows some α-Al dendrites and the inter-dendritic Chinese script BE-($Al_{15}(Fe,Mn)_3Si_2$ + α-Al) and BE-(Mg_2Si + α-Al). The inverse pole figure (IPF) image with misorientation angle (minimum 15 deg to maximum 65 deg) (in black line) shown in Figure 3(c) demonstrates that the α-Al in the BE-($Al_{15}(Fe,Mn)_3Si_2$ + α-Al) has a large misorientation (15 deg $< \varphi <$ 65 deg) with the adjacent primary α-Al dendrites. The BE-(Mg_2Si + α-Al) associated to BE-($Al_{15}(Fe,Mn)_3Si_2$ + α-Al) also has large misorientation (15 deg $< \varphi <$ 65 deg) with the surrounding primary α-Al dendrites.

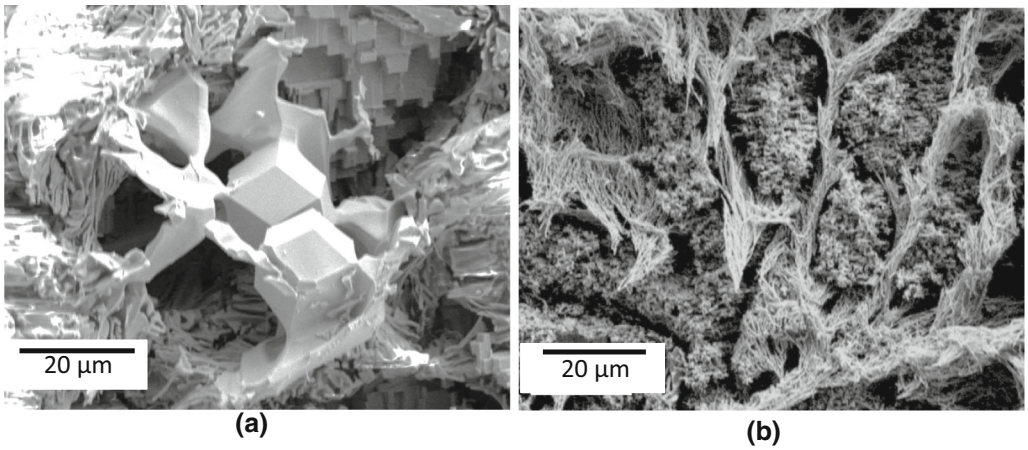

Fig. 2—SEM images showing the microstructure in 3D of Al-5Mg-2Si-0.4Mn-0.7Fe alloys solidified at 3.5 K/s with pouring temperature of (*a*) 690 °C indicating the BE-(FIMCs + α-Al) with Chinese script morphology connected and grown from the compacted primary FIMCs, and the BE-(Mg_2Si + α-Al) connected and grown from Chinese script FIMCs, and (*b*) 660 °C showing the TE-(FIMCs + Mg_2Si + α-Al) in the α-Al inter-dendrites zone with fine spacing and needle-like morphology.

Figures 3(a) through (c) show the EBSD mapping results of TE structure in α-Al inter-dendritic zone in sample that casted at 660 °C. Figure 3(a) shows the uniform TE-(FIMC + Mg_2Si + α-Al) structure in the α-Al inter-dendritic area. The IPF + IQ image in Figure 3(c) with the crystal lattice of α-Al in primary dendrites and TE structure shows that the α-Al phase in the TE structure has the same orientation as the α-Al phase in the associated primary α-Al dendrites.

Interface between $Al_{15}(Fe,Mn)_3Si_2$ and Mg_2Si was further examined by TEM, with an example being shown in Figure 4. Figure 4(a) shows the high-resolution TEM observation focused on the interface between the $Al_{15}(Fe,Mn)_3Si_2$ and Mg_2Si when the incident electron beam is parallel to [1 1 1] zone direction of $Al_{15}(Fe,Mn)_3Si_2$ (bottom part) and [1 1 1] zone direction of Mg_2Si (upperpart). It shows that the atomic interface between $Al_{15}(Fe,Mn)_3Si_2$ and Mg_2Si is sharped. The selected area electron diffraction (SAED) pattern in Figure 4(b) was taken from both the $Al_{15}(Fe,Mn)_3Si_2$ phase and the adjacent Mg_2Si with the incident electron beam being paralleled to [1 1 1] zone direction of $Al_{15}(Fe,Mn)_3Si_2$ and [1 1 1] zone direction of Mg_2Si. The indexed schematic diffraction patterns shown in Figure 4(c) suggested an orientation relationship (OR) between $Al_{15}(Fe,Mn)_3Si_2$ and Mg_2Si: $(\bar{1}01)Al_{15}(Fe,Mn)_3Si_2$ // $(\bar{2}\bar{4}6)Mg_2Si$ and $[111]Al_{15}(Fe,Mn)_3Si_2$ // $[111]Mg_2Si$.

According to the phase diagram calculation results, the main solidification sequence of the Al-5Mg-2Si-0.4Mn-0.7Fe alloy is primary $Al_{15}(Fe,Mn)_3Si_2$, BE-($Al_{15}(Fe,Mn)_3Si_2$ + α-Al), and TE-(α-Al + $Al_{13}Fe_4$ + Mg_2Si). When casted at 690 °C, five kinds of structures can be observed which are primary $Al_{15}(Fe,Mn)_3Si_2$, primary α-Al, BE-($Al_{15}(Fe,Mn)_3Si_2$ + α-Al), BE-(Mg_2Si + α-Al) and TE-(α-Al + $Al_{13}Fe_4$ + Mg_2Si). As we reported,[20] the BE structure Chinese script $Al_{15}(Fe,Mn)_3Si_2$ was nucleated and grown from the primary $Al_{15}(Fe,Mn)_3Si_2$ due to the lowest lattice misfit (0 pct)[22] between the solid and the substrate. In addition, the EBSD results in Figure 3(c) revealed that the α-Al in BE-($Al_{15}(Fe,Mn)_3Si_2$ + α-Al) does not have the same orientation as any associated primary α-Al. Therefore, the BE-($Al_{15}(Fe,Mn)_3Si_2$ + α-Al) is less possible to be nucleated on the surrounding primary α-Al with the α-Al as the leading phase. The BE-$Al_{15}(Fe,Mn)_3Si_2$ can be considered to be nucleated on the primary $Al_{15}(Fe,Mn)_3Si_2$ as the leading phase of the BE-($Al_{15}(Fe,Mn)_3Si_2$ + α-Al). The other work[22] has reported that the primary $Al_{15}(Fe,Mn)_3Si_2$ particles can act as the nucleation substrates for the following α-Al. The primary α-Al phase can be considered to be formed before the formation of BE-($Al_{15}(Fe,Mn)_3Si_2$ + α-Al) and after the formation of primary $Al_{15}(Fe,Mn)_3Si_2$ particles in this study. The other interesting result is that the large-scale Chinese script BE-(Mg_2Si + α-Al) is always associated with the BE-($Al_{15}(Fe,Mn)_3Si_2$ + α-Al). The 3D SEM image (Figure 2(a)) shows that the BE- Mg_2Si is connected firmly with the BE-$Al_{15}(Fe,Mn)_3Si_2$. The TEM results shown in Figure 4 revealed a well-defined orientation relationship (OR) between the $Al_{15}(Fe,Mn)_3Si_2$ and Mg_2Si. According to the previous study,[20] $Al_{15}(Fe,Mn)_3Si_2$ is {1 1 0} faceted. The examined interface (Figure 4(a)) between $Al_{15}(Fe,Mn)_3Si_2$ and Mg_2Si shows that the $Al_{15}(Fe,Mn)_3Si_2$ phase also has {1 1 0} faceted surface, but the Mg_2Si phase matches the Fe-IMC with high index plane. These results indicate that the $Al_{15}(Fe,Mn)_3Si_2$ is the nucleation substrate for the Mg_2Si. Therefore the Mg_2Si phase in the BE-(Mg_2Si + α-Al) structure is the leading phase which nucleates on the BE-$Al_{15}(Fe,Mn)_3Si_2$. Under this solidification condition, the solidification sequence is (1) primary $Al_{15}(Fe,Mn)_3Si_2$; (2) BE-($Al_{15}(Fe,Mn)_3Si_2$ + α-Al); (3) BE-(Mg_2Si + Al) and (4) TE-(α-Al + $Al_{13}Fe_4$ + Mg_2Si).

However, when the Al-5Mg-2Si-0.4Mn-0.7Fe alloy was casted at 660 °C, the primary $Al_{15}(Fe,Mn)_3Si_2$ phase was suppressed, and the primary α-Al became dominant. Then the large-scale Chinese script BE-

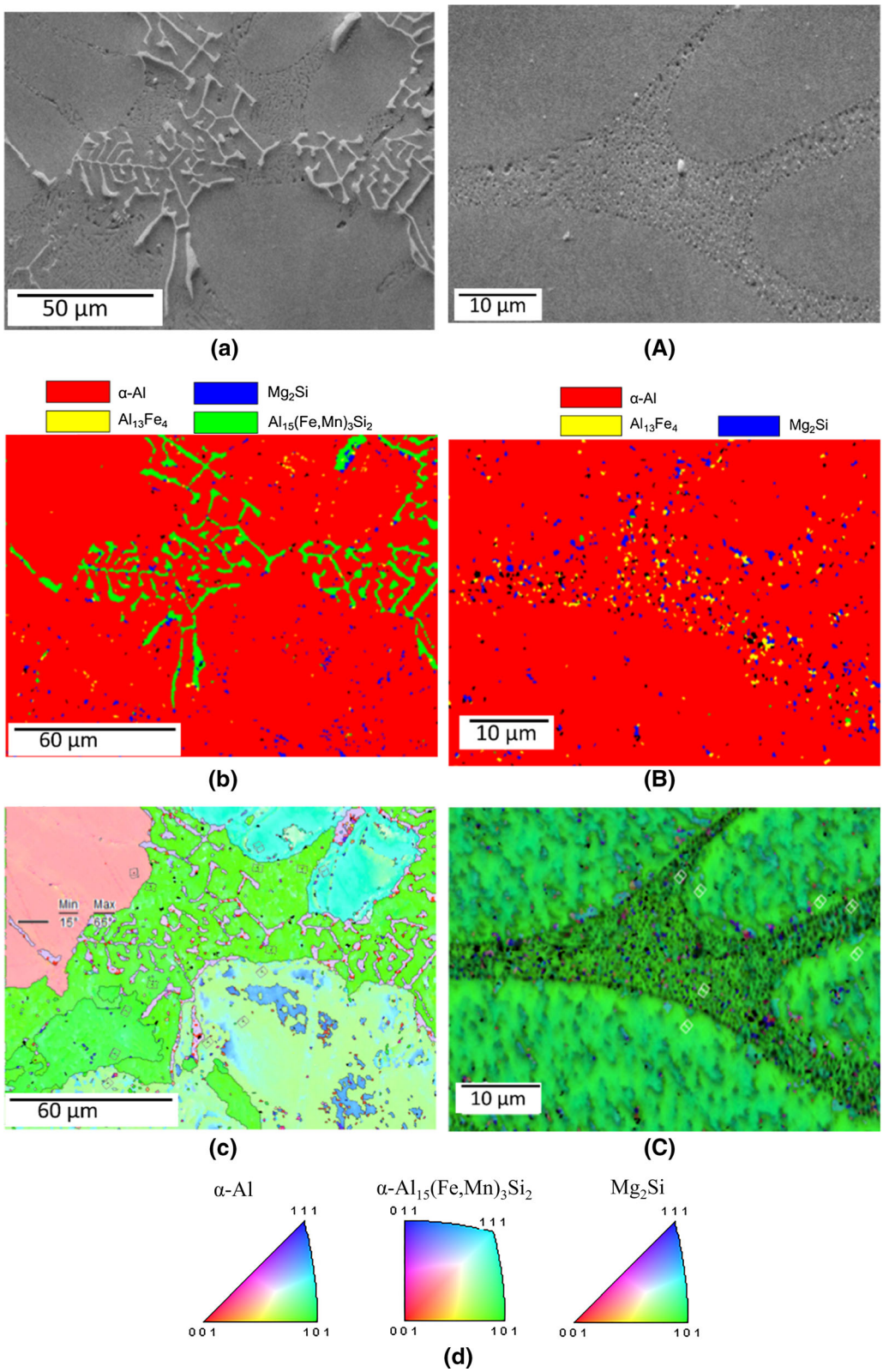

Fig. 3—EBSD map of Al-5Mg-2Si-0.4Mn-0.7Fe alloys solidified at 3.5 K/s with pouring temperature of (*a* to *c*) 690 °C, and (*a* through *c*) 660 °C, showing the eutectic structure in α-Al inter-dendritic zone with Chinese script BE-($Al_{15}(Fe,Mn)_3Si_2$ + α-Al): (*a*) SEM image, (*b*) phase image and (*c*) IPF image with crystal lattice and misorientation angle (minimum 15 deg to maximum 65 deg); and ternary eutectic in α-Al inter-dendritic zone: (*A*) SEM image, (*B*) phase image and (*C*) IPF + IQ image with crystal lattice, (*d*) IPF colour keys of phases.

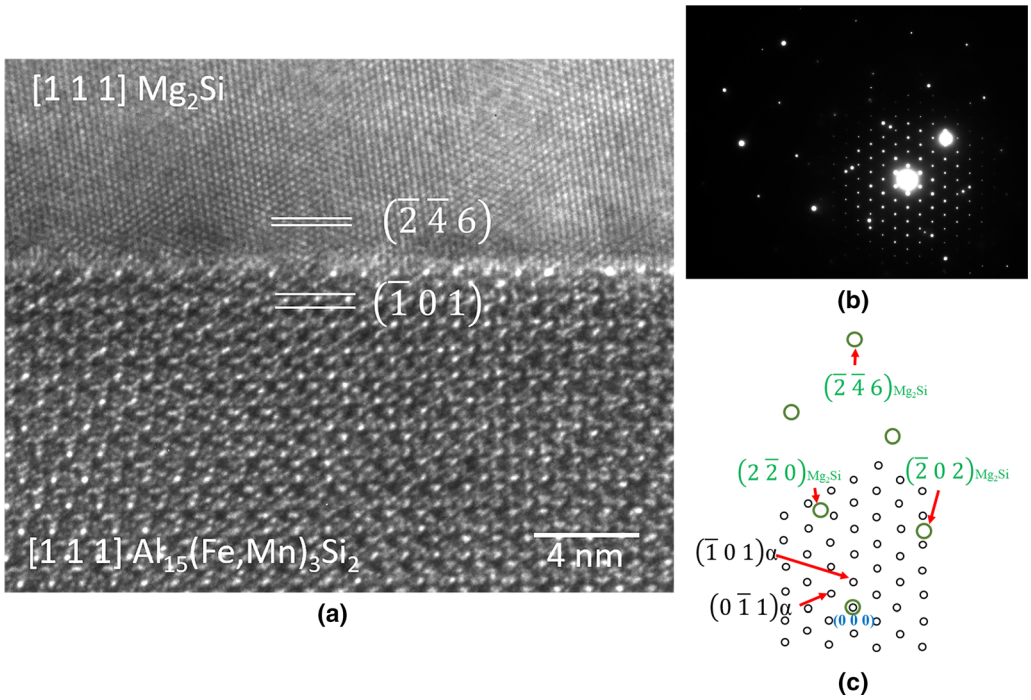

Fig. 4—(*a*) High-resolution TEM image of the interface of α-$Al_{15}(Fe,Mn)_3Si_2$ and Mg_2Si phase when viewed along the [1 1 1] zone direction of α-$Al_{15}(Fe,Mn)_3Si_2$ and [1 1 1] zone direction of Mg_2Si, (*b*) the selected area (SAED) diffraction pattern taken from the α-$Al_{15}(Fe,Mn)_3Si_2$ and Mg_2Si interface and (*c*) corresponding indexed schematic diffraction pattern of (*b*). These results suggest the following orientation relation (OR): $(\bar{1}01)Al_{15}(Fe,Mn)_3Si_2$ // $(\bar{2}\bar{4}6)Mg_2Si$ and $[111]Al_{15}(Fe,Mn)_3Si_2$// $[111]Mg_2Si$.

($Al_{15}(Fe,Mn)_3Si_2$ + α-Al) was suppressed correspondingly. This is possible due to the lack of the potent nucleation substrate for the BE-$Al_{15}(Fe,Mn)_3Si_2$ and BE-Mg_2Si. In this case, the remaining liquid in the α-Al inter-dendritic zone formed the TE-(FIMCs + Mg_2Si + α-Al). The EBSD map shown in Figure 3(C) revealed that the α-Al in TE-(FIMCs + Mg_2Si + α-Al) has the same orientation with the surrounding primary α-Al, which indicates that the TE-(FIMCs + Mg_2Si + α-Al) nucleates on the surrounding primary α-Al with the α-Al leading phase.

In addition, the morphology and eutectic spacing of the eutectic structures are found to depend on the leading phase. When the IMCs (FIMCs or Mg_2Si) were selected as the leading phase, the eutectic structure grew into large size structure, such as Chinese script BE-($Al_{15}(Fe,Mn)_3Si_2$ + α-Al) and BE-(Mg_2Si + α-Al) (Figures 1 and 2). When α-Al was selected as the leading phase, both the IMC and the eutectic structure was refined. (Figures 1 and 2).

In this study, BE-($Al_{15}(Fe,Mn)_3Si_2$ + α-Al) nucleated and grew from the primary $Al_{15}(Fe,Mn)_3Si_2$ phase with the BE-$Al_{15}(Fe,Mn)_3Si_2$ as the leading phase in Al-5Mg-2Si-0.4Mn-0.7Fe alloy when casted at 690 °C. The BE-(Mg_2Si + α-Al) nucleated on the $Al_{15}(Fe,Mn)_3Si_2$ phase in BE-($Al_{15}(Fe,Mn)_3Si_2$ + α-Al) structure with the Mg_2Si as the leading phase in Al-5Mg-2Si-0.4Mn-0.7Fe alloy when casted at 690 °C. The TE-(FIMCs + Mg_2Si + α-Al) nucleated on the surrounding primary α-Al. The α-Al was the leading phase for the TE structure in Al-5Mg-2Si-0.4Mn-0.7Fe alloy when casted at 660 °C. A well-defined orientation relationship between α-$Al_{15}(Fe,Mn)_3Si_2$ and Mg_2Si: $(\bar{1}01)[111]$α-$Al_{15}(Fe,Mn)_3Si_2$ // $(\bar{2}\bar{4}6)[111]$ Mg_2Si was observed.

The EPSRC is gratefully acknowledged for providing financial support under Grant EP/N007638/1.

OPEN ACCESS

REFERENCES

1. G.S. Cole and A.M. Sherman: *Mater. Charact.*, 1995, vol. 35, pp. 3–9.
2. T.O. Mbuya, B.O. Odera, and S.P. Nganga: *Int. J. Cast Metal Res.*, 2003, vol. 16, pp. 454–65.
3. M.A. Easton, M. Qian, A. Prasad, and D.H. StJohn: *Curr. Opin. Solid State Mater. Sci.*, 2016, vol. 20, pp. 13–24.
4. O. Engler and J. Hirsch: *Mater. Sci. Eng. A*, 2002, vol. 336, pp. 249–62.
5. A. Cibula: *J. Inst. Met.*, 1949–1950 vol. 76, pp. 321–360.
6. A. Cibula: *J. Inst. Met.*, 1951–1952, vol. 80, pp. 1–16.
7. R.O. Kaibyshev, I.A. Mazurina, and D.A. Gromov: *Met. Sci. Heat Treat.*, 2006, vol. 48 (2), pp. 14–19.
8. M.D. Eborall: *J. Inst. Met.*, 1949–1950, vol. 76, pp. 295–320.
9. Z. Fan, Y. Wang, Y. Zhang, T. Qin, X.R. Zhou, G.E. Thompson, T. Pennycook, and T. Hashimoto: *Acta Mater.*, 2015, vol. 84, pp. 292–304.
10. B.S. Murty, S.A. Kori, and M. Chakraborty: *Int. Mater. Rev.*, 2002, vol. 47, pp. 3–29.
11. M.C. Flemings: *Metall. Trans.*, 1974, vol. 5 (10), pp. 2121–34.
12. C.W. Schmidt, D. Mortensen, K.F. Karhausen: *Light Metals*, 2017, pp. 811–19.
13. M. Cooper: *Acta Cryst.*, 1967, vol. 23, pp. 1106–07.
14. V. Hansen, B.C. Hauback, M. Sundberg, C. Romming, J. Gjonnes: *Acta Cryst., Section B: Structural Science*, 1998, vol. 54, pp. 351-357.
15. C. Servant, F. d'Yvoire, and N. Rodier: *Acta Cryst., Sect. C*, 1995, vol. 51, pp. 177–79.
16. J. Grin, U. Burkhardt, M. Ellner, and K. Peters: *Z. Kristallogr.*, 1994, vol. 209, pp. 479–87.
17. R.N. Corby and P.J. Black: *Acta Cryst., Sect. B*, 1977, vol. 33, pp. 3468–75.
18. A.M.A Mohamed and F.H. Samuel: *Heat Treatment-Conventional and Novel Applications. 1st ed.,* Frank Czerwinski, Canada, 2012, Chapter 4, pp. 55–72.
19. X.P. Li, X.J. Wang, M. Saunders, A. Suvorova, L.C. Zhang, Y.J. Liu, M.H. Fang, and Z.H. Huang: *Acta Mater.*, 2015, vol. 95, pp. 74–82.
20. Z.P. Que, Y. Wang, and Z. Fan: *Metall. Mater. Trans. A*, 2018, vol. 49A, pp. 2173–81.
21. Standard Test Procedure for Aluminum Alloy Grain Refiners: TP-1, *The Aluminum Association*, Washington DC, 1987.22. Z. Fan: *Metall. Mater. Trans. A*, 2013, vol. 44A, pp. 1409–18.
22. W. Yang, S. Ji, X. Zhou, I. Stone, G. Scamans, G.E. Thompson, and Z. Fan: *Metall. Mater. Trans. A*, 2014, vol. 45A, pp. 3971–80.